Temperature induced in human organs due to near-field and far-field electromagnetic exposure effects

Teerapot Wessapan [a], Phadungsak Rattanadecho [b,*]

[a] School of Aviation, Eastern Asia University, Pathumthani 12110, Thailand
[b] Center of Excellence in Electromagnetic Energy Utilization in Engineering (CEEE), Department of Mechanical Engineering, Faculty of Engineering, Thammasat University (Rangsit Campus), Pathumthani 12120, Thailand

ABSTRACT

The main biological effect from exposure to electromagnetic (EM) radiation is a temperature rise in the human body and its sensitive organs, which results from absorbing electromagnetic field (EMF) power. EM near-field and far-field sources, which have different operating frequencies and exposure distances, result in different EMF distribution patterns and EMF power absorptions by the human body. Actually, the severity of the physiological effect can occur with small temperature increases in the sensitive organs. However, the EM absorption characteristics and the temperature increase distribution resulting from different field radiation patterns from EM sources are not well established. To adequately explain the biological effects that are associated with the EMF energy absorption, a systematic study of different EMF distribution patterns and how they interact with body tissue is needed. This study considers the computationally determined specific absorption rate (SAR) and the heat transfer in a heterogeneous human torso model with internal organs exposed to near-field and far-field EM radiations at different frequencies. The electric field, SAR, and the temperature distributions in various organs during exposure to EMFs are obtained through the numerical simulation of EM wave propagation and an unsteady bioheat transfer model. The findings indicate that the field radiation pattern and the operating frequency of an EM source significantly influence the electric field, the SAR, and the temperature distribution in each organ. Moreover, the tissue's dielectric properties also affect the temperature distribution patterns within the body tissue. These findings enable researchers to more accurately determine the exposure limits for the power output of wireless transmitters, and the distance that they should remain from the humans.

© 2017 Published by Elsevier Ltd.

1. Introduction

In recent years, there has been increasing public concern about the influence of EM waves on the human body. At present, humans are exposed to various EMF sources in many situations that occur in everyday life. The utilization of EM waves in various applications has been increasing rapidly, and includes use in mobile phones, tablet, laptops, as well as mobile phone base stations. EM near-field and far-field sources have different power levels and exposure distances that cause difference EMF distribution patterns and EMF power absorptions by the human body. Although safety standards, in terms of the maximum SAR values, are regulated [1], they are not explicitly stated in terms of the maximum temperature increase in tissue caused by EM energy absorption, which is the actual influence of the dominant factors that induce adverse physiological effects. It is known that the main short-term biological effect from exposure to EM radiation is the temperature rise in the human body and its sensitive organs from EM power absorption. Some significant thermal damage can occur in sensitive tissues under the condition of partial-body exposure to intense EM waves [2,3].The severity of the physiological effect can occur through a small temperature increase in a sensitive organ. An increase of approximately 1–5 °C in the human body temperature can cause numerous malformations, temporary infertility in males, brain lesions, and blood chemistry changes. Even a small temperature increase of approximately 1 °C in the human body can lead to the altered production of hormones and a suppressed immune response [4].

However, in realistic situations, the temperature increase cannot be directly measured in the body. Instead, it must be found indirectly through numerical techniques. Therefore, the numerical analysis of heat transfer in human body organs exposed to EM

Nomenclature

C	specific heat capacity (J/(kg K))		ε	permittivity (F/m)
E	electric field intensity (V/m)		σ	electric conductivity (S/m)
f	frequency of incident wave (Hz)		ω	angular frequency (rad/s)
H	magnetic field (A/m)		ρ	density (kg/m^3)
h	convection coefficient (W/m^2·K)		ω_b	blood perfusion rate (1/s)
j	current density (A/m^2)			
k	thermal conductivity (W/(m K))		*Subscripts*	
n	normal vector		b	blood
Q	heat source (W/m^3)		ext	external
T	temperature (K)		met	metabolic
t	time		r	relative
			0	free space, initial condition
Greek letters				
μ	magnetic permeability (H/m)			

fields will provide useful information on the absorption of EM energy under a variety of exposure conditions. The thermal modeling of human tissue is important as a tool to investigate the effect of external heat sources, and to predict abnormalities in tissues. The modeling of heat transport in human tissue was first introduced by Pennes [5,6] based on the heat diffusion equation. The equation is normally called Pennes bioheat equation and it is frequently used for the analysis of heat transfer in human tissues. Due to simplifications of the Pennes bioheat model, other researchers have established mathematical bioheat model by extending or modifying the Pennes model [7–9]. Although many advanced transport models of biological tissue have been proposed, Pennes bioheat model is still a good approximation and it is still widely used for modeling the heating of biological tissue because of its easy implementation and its minimal data requirement. There are some experimental studies in animals, such as in rats [10], cows [11], and pigs [12]. However, the results may not represent the practical transport processes that occur in human tissues. Calculating the spatially-induced electric field, the SAR, and the temperature increase becomes more complex when the human body is non-uniform in shape and contains several organs. Most studies of the human body's exposure to EM waves have not considered a realistic domain with complicated organs made from several types of tissues [2,13,14], and experimental validation is limited or non-existent. Our research group has numerically investigated the temperature increase in human tissue subjected to EMFs in various situations [15–27]. Wessapan et al. [15,16] utilized a 2D finite element method (FEM) to obtain the SAR and the temperature increase in a human body exposed to leaked EM waves. Wessapan et al. [17,18] developed a 3D model of the human head to investigate the SAR and the temperature distributions in the human head during exposure to mobile phone radiation. Keangin et al. [19,20] carried out a numerical simulation of liver cancer that was treated using a complete mathematical model that considered a coupled model that described EM wave propagation and heat transfer. Moreover, an analysis of mechanical deformation in the biological tissues from microwave ablation was investigated [21]. Wessapan et al. [22–26] investigated the SAR and the temperature distributions in the eye during exposure to EM waves based on porous media theory. The increased testicular temperature induced by EMFs was also investigated [27]. However, the EM absorption characteristics and the temperature increase distributions in the body that resulted from different field radiation patterns from EM near-field and far-field sources are not well established. To adequately explain the biological effects, which are associated with

the EMF energy absorption, a systematic study of different EMF distribution patterns that interact with body tissues is necessary.

This study presents the computational determination of the SAR and temperature increases in a human torso exposed to near-field and far-field EM radiations. The work described in this paper is substantially extended from our previous work by further enhancing the focus on the effect of the EMF distribution patterns under near-field and far-field conditions. A heterogeneous human torso model is developed to determine the SAR and the temperature increases induced by EM energy. The heterogeneous human model comprises eleven types of tissue: the skin, fat, muscle, bone, testis, the large intestine, the small intestine, bladder, blood, stomach, and the liver. The model excludes the presence of clothing to ease the modeling procedures. The electric field, the SAR, and the temperature increase distributions in various organs during exposure to EMFs are obtained through numerical simulation of EM wave propagation and an unsteady bioheat transfer model. The effect of the exposure distance on the SAR and the temperature increases in each tissue organ is systematically investigated. In particular, the maximum SAR and temperature increase in the internal organs are compared for near-field and far-field exposure. The frequencies of 900 and 1800 MHz are chosen for this study as these frequencies are used globally in a wide range of applications that include Global Systems for Mobile Communications (GSM) services. Attention is paid to the maximum SAR and temperature increase in a body's organs with respect to the safety guidelines to consider the possible consequences of EM exposure and their implications for hazard thresholds.

2. Formulation of the problem

Concerns about the influence of an EM wave on the human body have focused mainly on the temperature increases in a human body and head due to mobile device exposure in the near-field region, but other types of illnesses have also been linked with over exposure to far-field radiation from high-power base stations. EM near-field and far-field sources have different power levels and exposure distances that cause differences in the resulting EMF distribution pattern and EMF power absorption in the human body. However, the EM absorption characteristics and the temperature increase distributions that result from different field radiation patterns from EM sources are not well established. To adequately explain the biological effects, which are associated with the EMF energy absorption, a systematic study of different EMF distribution patterns that interact with body tissue is needed.
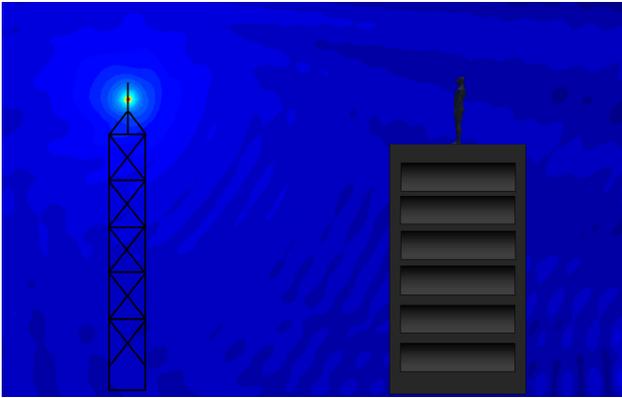
Fig. 1. Human exposure to EM radiations from from near-field and far-field sources.

Fig. 1 shows human exposure to EM radiation in both the near-field and far-field ranges. Due to ethical considerations, the exposure of humans to EM fields, for experimental purposes, is limited. It is more convenient to develop a realistic human model through numerical simulation. A highlight of this work is the illustration of heat transfer in a heterogeneous human torso model with internal organs that were exposed to near-field and far-field EM radiation with different frequencies. The analyses of the electric field, the SAR, and the temperature increase in the model will be discussed in Section 3.

3. Methods and the model

The aim of this study is to investigate the interaction effects between EMFs and human body tissues that occur during exposure to near-field and far-field EM radiation. Fig. 2 shows the physical representation of this study, where interactions between the human body and a dipole antenna takes place. The first step in evaluating the effects of a certain exposure to EM fields in the human body is to determine the induced internal EM fields and their spatial distribution. Thereafter, the EM energy absorption, which results in a temperature increase in each organ, and other interactions, can be considered.

3.1. Physical model

To investigate the effect of the exposure distance on the SAR and the temperature increase in each tissue organ, a heterogeneous human torso model is exposed to an electric dipole antenna. In this study, a 2D model is considered to minimize the amount of computational time while maintaining resolution [15]. The heterogeneous human torso model has a dimension of 400 mm in width and 525 mm in height. This model is comprised of eleven types of tissues: the skin, fat, muscle, bone, testis, the large intestine, the small intestine, bladder, blood, stomach and the liver. These tissues have different dielectric and thermal properties. The dielectric and thermal properties of the tissues are obtained according to the comprehensive literature review of Hasgall [28] (www.itis.ethz.ch/database), and are given in Tables 1 and 2 respectively. Each tissue is assumed to be homogeneous, as well as electrically and thermally isotropic. There is no effect on the chemical reaction and phase change within the tissue. The antenna's feed point is located in front of the abdominal segment with different distances. The antenna is excited at the center feed point, and the transmitted power is determined as the complex product of the current and voltage at the feed point. The antenna transmits various radiated powers with the frequencies of 900 and 1800 MHz.

3.2. Equations for EM wave propagation analysis

The mathematical models illustrate the electric field and its variations and relate them to the physiological phenomena that arise from the interactions between electromagnetic fields and biological tissues. To simplify the problem, the following assumptions are made:

1. The EM wave propagation is modeled in two dimensions.
2. The EM wave interaction with the tissue proceeds in the open region.
3. The free space is truncated by a scattering boundary condition.
4. The model assumes that the dielectric properties of each tissue are constant.
5. The radiated waves from the dipole are characterized by transverse electric (TE) fields.

To describe the propagation of electromagnetic waves through a medium, the EM wave propagation is calculated using Maxwell equations [16], which mathematically describes the interdependence of the EM waves. The general form of Maxwell equations is simplified to demonstrate the EM field that penetrates into the tissue as follows:

$$\nabla \times \left(\frac{1}{\mu_r} \nabla \times E \right) - k_0^2 \left(\varepsilon_r - \frac{j\sigma}{\omega\varepsilon_0} \right) E = 0 \qquad (1)$$

$$\varepsilon_r = n^2 \qquad (2)$$

where E is the electric field intensity (V/m), μ_r is the relative magnetic permeability, n is the refractive index, ε_r is the relative dielectric constant, $\varepsilon_0 = 8.8542 \times 10^{-12}$ F/m is the permittivity of free space, σ is the electric conductivity (S/m), $j = \sqrt{-1}$, and k_0 is the free space wave number (m^{-1}).

3.2.1. Boundary condition for wave propagation analysis

The boundary conditions along the interfaces between different mediums, namely, between air and tissue, are considered as a continuity boundary condition:

$$n \times (H_1 - H_2) = 0 \qquad (3)$$

The outer sides of the calculated domain, i.e., the free space, are considered as a scattering boundary condition to eliminate reflections:

$$n \times (\nabla \times E) - jkE = 0 \qquad (4)$$

where k is the wave number (m^{-1}), n is the normal vector, $j = \sqrt{-1}$, and H is the magnetic field (A/m).

3.3. Interaction of EM fields and human tissues

When the EM waves propagate through a tissue, the energy of the EM waves is absorbed by the tissue. The SAR is defined as the power dissipation rate normalized by the material density. The SAR is given by:

$$SAR = \frac{\sigma}{\rho} |E|^2 \qquad (5)$$

where E is the electric field intensity (V/m), σ is the electric conductivity (S/m), and ρ is the tissue density (kg/m^3).

3.4. Equations for heat transfer analysis

This study considers the heat transfer and temperature increases due to near-field and far-field exposures and their implications for the threshold for EM hazards. To solve the thermal
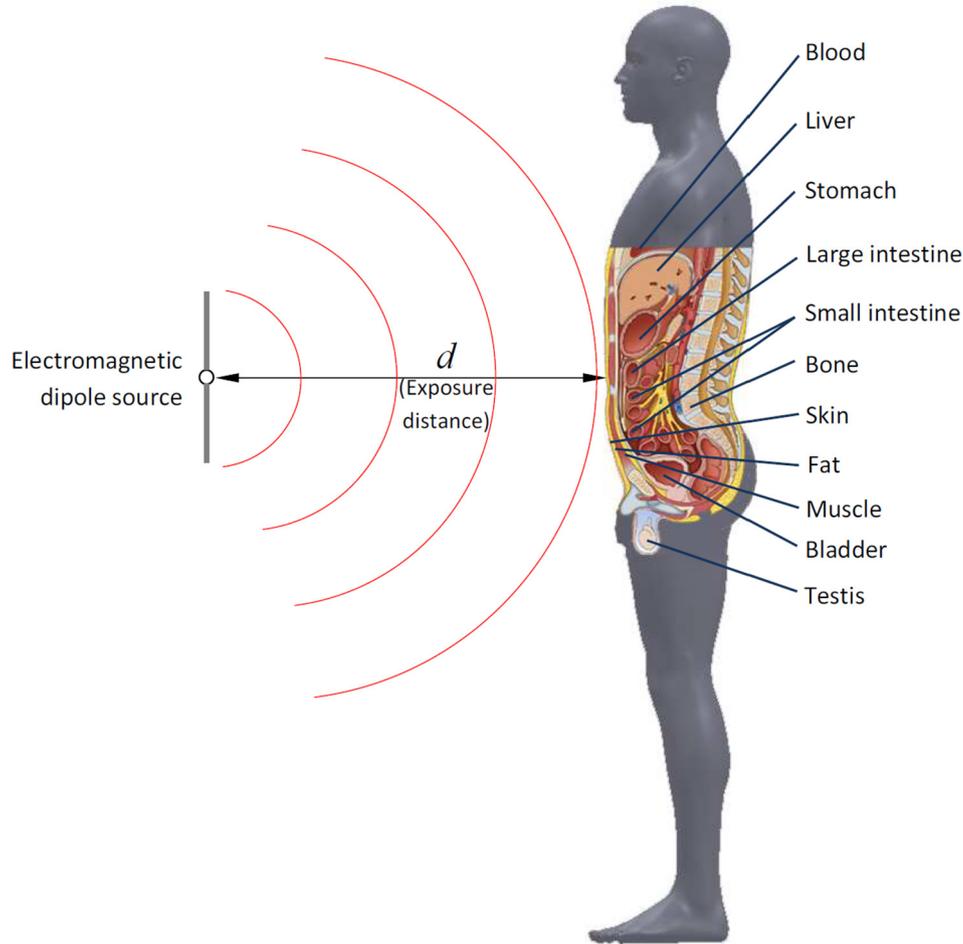
Fig. 2. The physical domain of the problem.

Table 1
Dielectric properties of tissues [28].

	900 MHz		1800 MHz	
	ε_r	σ (S/m)	ε_r	σ (S/m)
Skin	41.4	0.867	38.9	1.18
Fat	11.3	0.109	11.0	0.19
Muscle	55.0	0.943	53.5	1.34
Bone	12.5	0.143	11.8	0.275
Testis	60.6	1.21	58.6	1.69
Large intestine	57.9	1.08	55.1	1.58
Small intestine	59.5	2.17	55.9	2.7
Bladder	18.9	0.383	18.3	0.535
Blood	61.4	1.54	59.4	2.04
Stomach	65.1	1.19	63.2	1.70
Liver	46.8	0.855	44.2	1.29

problem, the coupled effects of the EM wave propagation and the unsteady bioheat transfer are investigated. The temperature distribution corresponds to the SAR. This is because the SAR, in the tissue, is distributed owing to energy absorption. Thereafter, the absorbed electromagnetic energy is converted to thermal energy, which increases the tissue's temperature. To reduce the complexity of the problem, the following assumptions are made:

1. The tissue is a bio-material with constant thermal properties.
2. There is no phase change for any substance in the tissue.
3. There are no chemical reactions in the tissue.
4. The heat transfer is modeled in two dimensions.
5. The thermal properties of the tissues are constant.

The temperature increase in the body's organs is obtained by solving Pennes bio-heat equation [5,6]. The transient bioheat equation effectively describes how heat transfer occurs within the tissue, and the equation can be written as:

$$\rho C \frac{\partial T}{\partial t} = \nabla \cdot (k \nabla T) + \rho_b C_b \omega_b (T_b - T) + Q_{met} + Q_{ext} \quad (6)$$

where ρ is the tissue density (kg/m³), C is the heat capacity of the tissue(J/kg K), k is the thermal conductivity of the tissue(W/m K), T is the tissue temperature (°C), T_b is the temperature of the blood (°C), ρ_b is the density of the blood(kg/m³), C_b is the heat capacity of the blood (J/kg K), ω_b is the blood perfusion rate (1/s), Q_{met} is the metabolic heat source (W/ m³), and Q_{ext} is the external heat source (the electromagnetic heat-source density) (W/ m³).

In this analysis, heat conduction between the tissue and the blood flow is approximated by the blood perfusion term, $\rho_b C_b \omega_b (T_b - T)$.

The external heat source term is equal to the resistive heat generated by an electromagnetic field (the electromagnetic power absorbed), which is defined as:

$$Q_{ext} = \frac{1}{2} \sigma_{tissue} |\bar{E}|^2 = \frac{\rho}{2} \cdot SAR \quad (7)$$

3.4.1. Boundary condition for the heat transfer analysis

The heat transfer analysis excludes the surrounding space and is considered only in the human model. The skin surface, as shown in Fig. 3, is considered under the convective boundary condition,

Table 2
Thermal properties of tissues [28].

Tissue	ρ (Kg/m^3)	k (W/m °C)	C (J/kg °C)	Q_{met} (W/m^3)	ω_b (1/s)
Skin	1109	0.37	3391	1829	0.001855
Fat	911	0.21	2348	464.6	0.0005775
Muscle	1090	0.49	3421	991.9	0.0006475
Bone	1908	0.32	1313	286.2	0.000175
Testis	1082	0.52	3778	3343.38	0.0035
Large intestine	1088	0.54	3655	12892.8	0.0133875
Small intestine	1030	0.49	3595	16366.7	0.017955
Bladder	1086	0.52	3581	1314.06	0.001365
Blood	1050	0.52	3617	–	–
Stomach	1088	0.53	3690	7757.44	0.00805
Liver	1079	0.52	3540	10714	0.01505

where the convection heat transfer coefficient between the skin and the air is 20 W/m^2·K.

$$-n \cdot (-k\nabla T) = h_{am}(T - T_{am}) \qquad (8)$$

where T_{am} is the ambient temperature (°C), and h_{am} is the convection coefficient (W/m^2·K).

It is assumed that no contact resistance occurs between the internal organs of the human body. Therefore, the internal boundaries are assumed to be continuous:

$$n \cdot (k_u \nabla T_u - k_d \nabla T_d) = 0 \qquad (9)$$

$$T_u = T_d \qquad (10)$$

At the initial stage, the temperature distribution within the human body is assumed to be uniform at 37 °C. Therefore, the temperature boundary condition of 37 °C is applied to the top and bottom surfaces, where the human torso model is truncated.
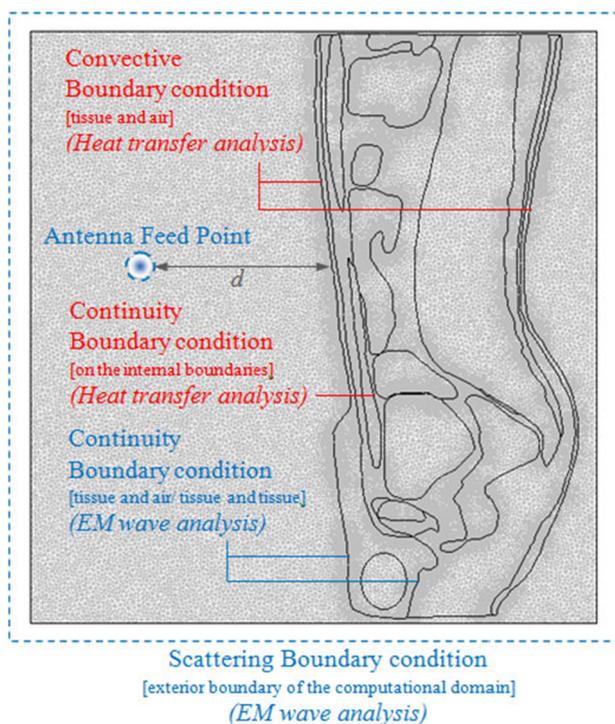
Fig. 3. A finite-element-mesh-based computational model and the boundary condition for analyzing EM wave propagation and heat transfer.

3.5. Calculation procedure

The electric field, the SAR, and the temperature distributions in the body's organs during exposure to EMFs are obtained through finite element formulations of the coupled electromagnetic–bioheat transfer model. The 2D model is discretized using triangular elements and the Lagrange quadratic elements are used to approximate the temperature and SAR variations across each element. This study uses a variable mesh method to solve the coupled problem. To obtain a good approximation, a fine mesh is specified in the sensitive are as shown in Fig. 3. The system of governing equations, as well as the initial and boundary conditions are solved numerically using the finite element method (FEM) via COMSOL™ Multiphysics to demonstrate the phenomenon that occurs in the organs exposed to EM fields. A grid independence test is carried out to identify the appropriate number of elements that are required. This grid independence test led to a mesh with approximately 160,000 elements. It is reasonable to assume that, with this element number, the accuracy of the simulation results will be independent of the number of elements.

4. Results and discussion

The electric field, SAR and temperature distributions in various organs during exposure to EMFs are obtained by numerical simulation of EM wave propagation and an unsteady bioheat transfer model. The dielectric and thermal properties are taken directly from Tables 1 and 2 respectively. The exposure condition considered in this study refers to the International Commission of Non-Ionizing Radiation Protection (ICNIRP) standard for safety levels at the maximum SAR value of 2 W/kg (general public exposure) and 10 W/kg (occupational exposure) [1]. The effect of exposure distance on the SAR and temperature increases in the heterogeneous human torso model with internal organs exposed to near-field and far-field EM radiations at different frequencies is systematically investigated. Numerically obtained data on the energy absorbed and temperature induced in the human torso model exposed to EMFs at 900 and 1800 MHz have been compared for the near and far-field exposures.

4.1. Verification of the model

To verify the accuracy of the present numerical models, the simulated results are validated against the numerical results obtained with the same geometric model used by Riu and Foster [13]. The SAR is determined in a homogeneous tissue model from near-field exposure to a dipole antenna. In the validation case, the dipole used operates at a frequency of 900 MHz and it transmits a radiated power of 0.6 W. The result of the validation test case is illustrated in Fig. 4, and it clearly shows good agreement of the SAR value of the tissue between the present solution and that found

by Riu and Foster [13]. The SAR decreases exponentially in the direction of wave propagation. This favorable comparison lends confidence to the accuracy of the present numerical model, and it ensures that the numerical model can accurately represent the phenomena occurring during the interaction of the EM fields with the tissues.

4.2. Comparison between near-field and far-field exposures

The near-field and far-field are regions of the EM field that are around a transmitting antenna or a radiation-emitting object. According to the radiation zone field, the far-field carries a relatively uniform wave pattern. In contrast, the near-field refers to regions where the propagation of electromagnetic waves has interference. In daily life, EMF exposures often take place in the near-field situation, such as with a mobile phone, and most of the reported studies on EMF exposure report results for near-field effects. The use of near-field data for predicting human risk from far-field exposure situations introduces errors. Due to ethical considerations, exposing a human to EM near-field and far-field radiation for experimental purposes is limited; however, a state-of-the-art technique is made possible via numerical simulation. In this study, the heterogeneous human torso model with internal

(a)

(b)

Fig. 4. Validation of the mathematical model: (a) the computational domain for validation; (b) comparison of the calculated SAR distribution with the SAR distribution obtained by Riu and Foster [13].

organs was exposed to near-field and far-field EM radiation. In the case of far-field exposure, the antenna's feed point was placed at a sufficiently large distance to ensure far-field conditions. The antenna's feed point is located in front of the abdominal segment at distances of 0.1 m and 10 m for near-field and far-field conditions respectively. The antenna used operates at 900 MHz frequency and transmits a radiated power of 1.0 W in the near-field and 100 W in the far-field. These are typical power levels for general mobile phones and high-power base stations.

Both near-field and far-field exposures produce highly non uniform spatial patterns in terms of their electric field intensities. Fig. 5 shows the simulation for an electric field distribution, within the framework of the model, resulting from exposure to the dipole antenna, which operates at a frequency of 900 MHz under near-field and far-field conditions. Due to the different dielectric characteristics of the various tissue layers, a different fraction of supplied EM energy will be absorbed by each layer in the model. Consequently, the reflection and transmission components of each layer contribute to the resonance of the standing wave in the tissue. The highest values for the electric fields occur in the outer area of the body, especially in the skin, directly beneath the feed point of the dipole antenna in front of the abdominal segment. By comparison, the maximum electric field intensity in the outer parts of the body, in the case of near-field exposure, displays a slightly higher value than in the case of far-field exposure. The maximum electric field intensities are 98.905 and 97.597 V/m for the near-field and far-field respectively. For both cases, the electric fields deep inside the body are extinguished as the electric fields are attenuated due to the absorbed EM energy, which is converted to heat. The EM absorption pattern in the case of near-field exposure typically differs significantly from the pattern that occurs in the case of far-field exposure. In the human model, which is closed to the dipole antenna in the near-field case (Fig. 5a), the electric field pattern is distributed in a nearly circular shape. For large distances in the case of far-field exposure (Fig. 5b), the electric field distribution pattern is similar to plane wave exposure.

Fig. 6 shows the SAR distribution, which is evaluated for the vertical cross-section of the human model that was exposed to an EM frequency of 900 MHz. It is evident from the figures that the results of the SAR distribution in the human body (Fig. 6) increased in a manner that corresponded with the electric field distribution (Fig. 5). Besides the electric field intensity, the magnitude of the electric conductivity (σ) and the tissue density (ρ), will directly affect the amount of SAR within the human body. This is because the SAR is a function of the electrical conductivity, which corresponds to Eq. (5). For both cases, the highest SAR values are obtained for the skin's surface. The maximum SAR values for near-field and far-field exposures are 3.824 and 3.723 W/kg respectively. The highest SAR values are obtained for the penis and the skin's surface. The main reason is that the penis and the skin are exposed to EMF radiation where the electric field intensity is strongest. Moreover, the penis and the skin have a high dielectric constant value (ε), which means that the propagating EM energy can be absorbed, which produces localized heating. Compared to the ICNIRP standard [1] for safety, a maximum SAR value of 2 W/kg (general public exposure) is recommended; the resulting SAR values for both the near-field and far-field are higher than the ICNIRP exposure limits for the general public exposure, and they are lower than the occupational exposure limit of 10 W/kg.

Exposure in the near-field results in very little energy deposition in the upper abdomen, the chest, and the thigh, which is understandable in view of the location of the antennas, which are in front of the middle abdominal segment. Some energy is deposited in the lower torso and in the legs for near-field exposure, but only a relatively small amount compared to the far-field case. The highest SAR value for the near-field and the far-field exposures
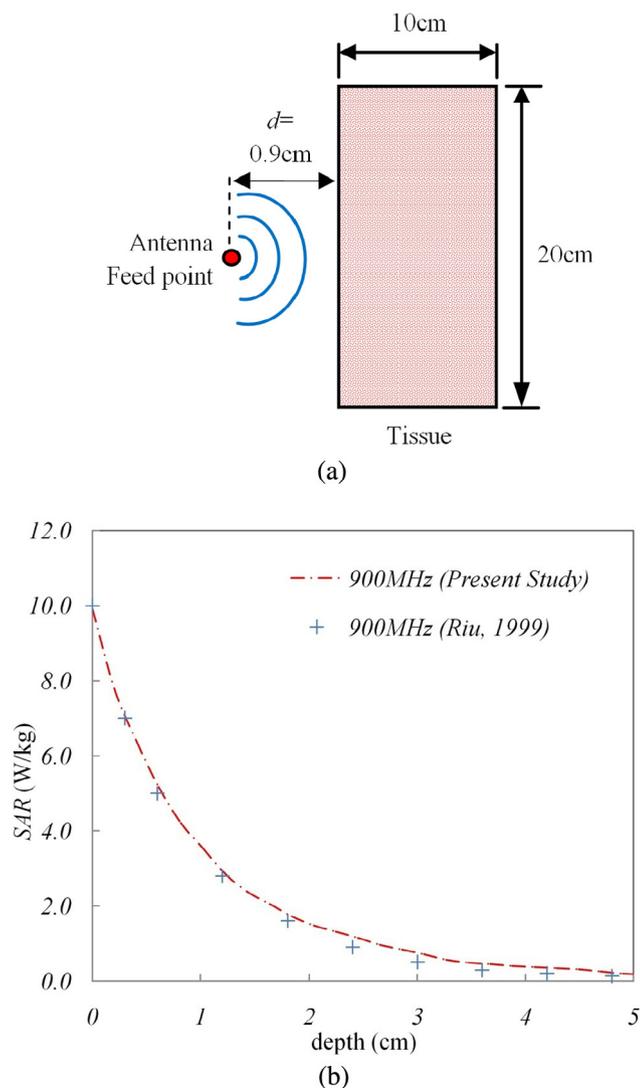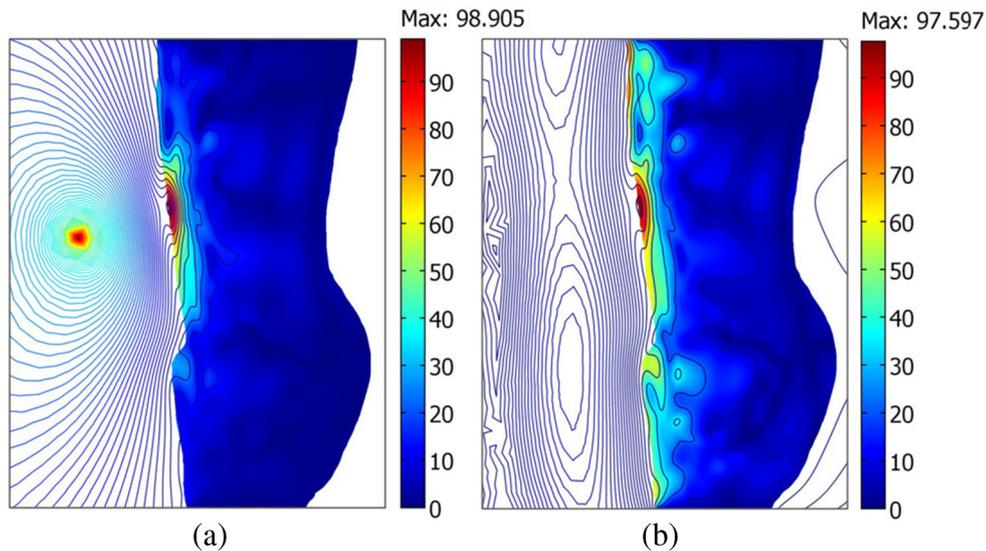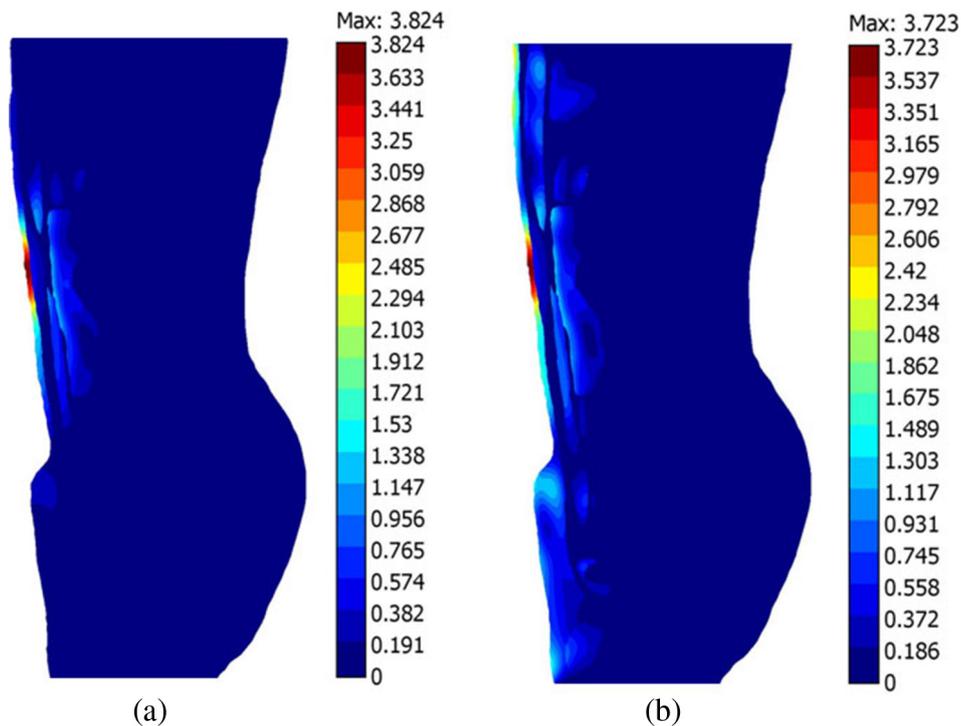
Fig. 5. Electric field distribution (V/m) in the human model during exposure to a dipole antenna. (a) 1 W at a distance of 0.1 m (near-field). (b) 100 W at a distance of 10 m (far-field).

Fig. 6. SAR distribution (W/kg) in the human model during exposure to a dipole antenna: (a) 1 W at a distance of 0.1 m (near-field), (b) 100 W at a distance of 10 m (far-field).

are almost the same, but the high absorption value in the near-field occurs only near the antenna axis (Fig. 6). In the near-field, as for the maximum value, the smaller input power of 1 W to the antenna (Figs. 5a and 6a) results in the same electric field intensity and SAR as when 100 W of power (Figs. 5b and 6b) is used in the far-field case. It should also be noted that an input power about 100 times higher than the maximum value for the far-field case is needed to obtain the same SAR found for the near-field case.

This study has focused on the temperature induced in human organs due to near-field and far-field EM exposure effects. In the heterogeneous human model, the effects of ambient temperature variation have been neglected to gain insight into the interactions between the EM fields and the tissues. At the skin's surface in the human model, the convective boundary condition is applied. The effect of thermoregulation mechanisms has also been neglected due to the small temperature increase that occurs during the exposure process. To investigate the temperature induced in human organs, the coupled effects of EM wave propagation and unsteady heat transfer, as well as the initial and boundary conditions are solved numerically. Due to these coupled effects, the electric field distribution in Fig. 5 and the SAR distribution in Fig. 6 are transformed into an incremental temperature increase in the tissues. Fig. 7 shows the steady state temperature increase in the vertical cross-section of the human model exposed to near-field (Fig. 7a)
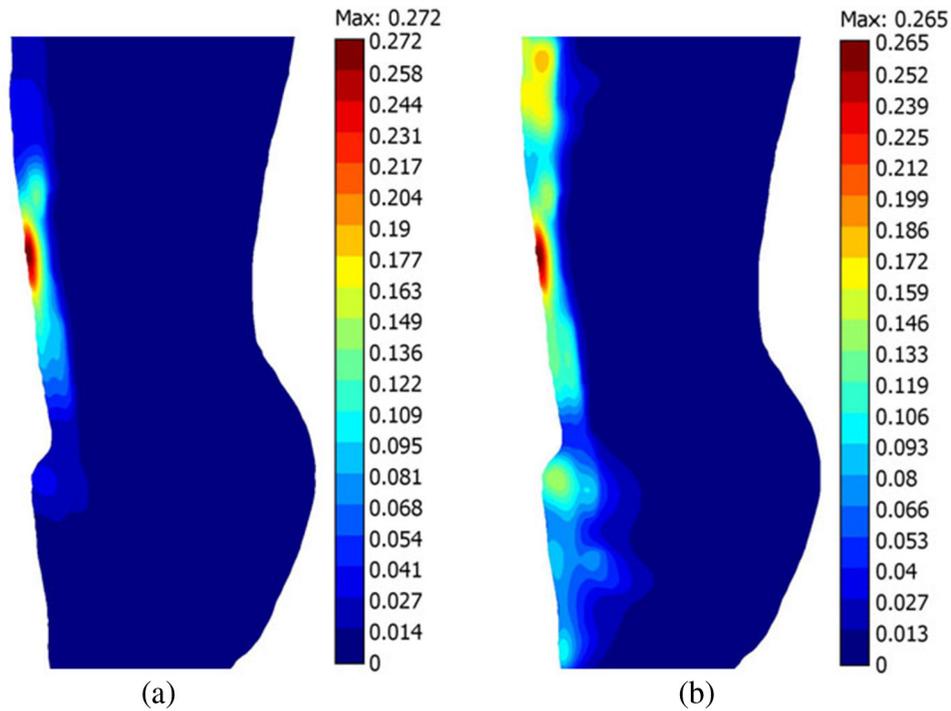
Fig. 7. Temperature increase distribution (°C) in the human model during exposure to a dipole antenna: (a) 1 W at a distance of 0.1 m (near-field) and (b) 100 W at a distance of 10 m (far-field).
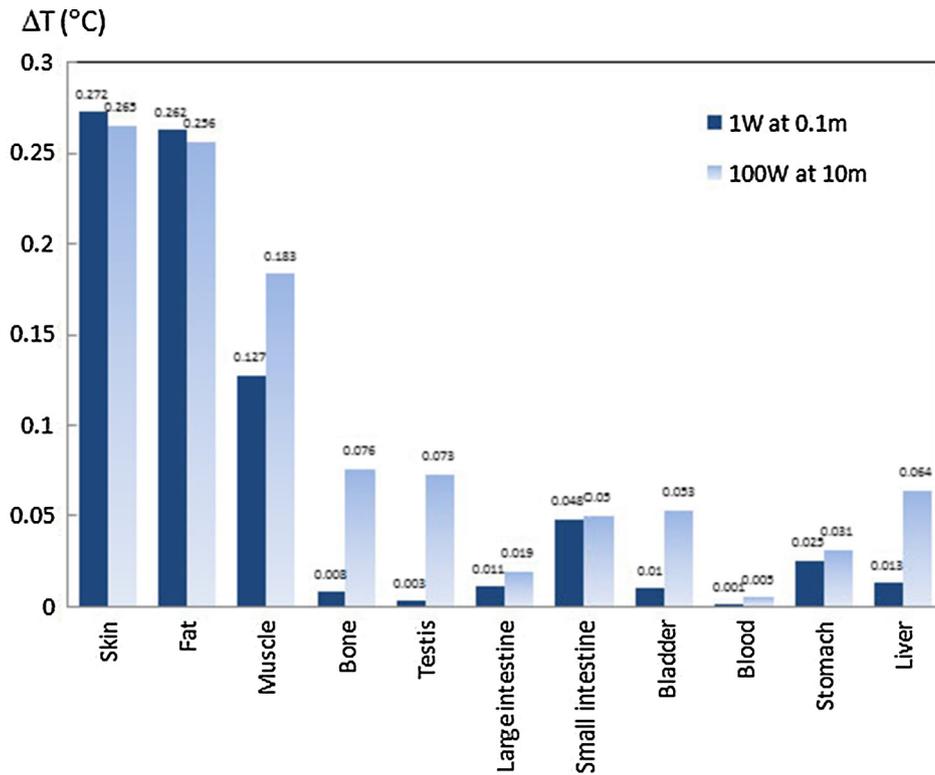

Fig. 8. Comparison of the temperature increase (°C) in each tissue type for a radiated power of 1 W, at distance of 0.1 m, and 100 W at a distance of 10 m for near and far-field sources.

and far-field (Fig. 7b) EMFs. For the model exposed for a longer amount of time to EMFs, the tissue temperature (Fig. 7) increased in accordance with the SAR (Fig. 6). This is because the electric fields in the tissue were attenuated owing to the energy absorbed, and thereafter, the absorbed energy is converted to thermal energy, which increases the body's temperature. Under a steady state, the maximum temperature increases are 0.272 °C and 0.265 °C for near-field and far-field exposures respectively.
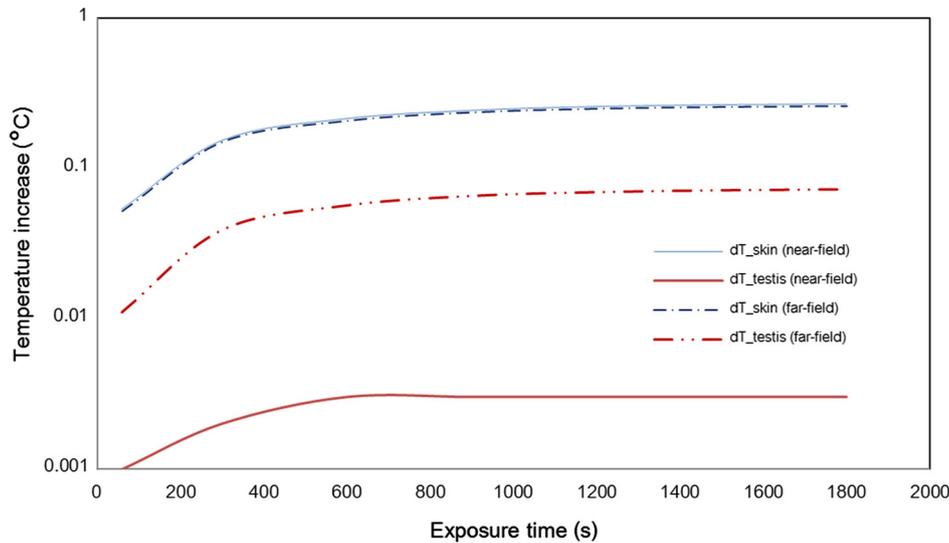
Fig. 9. Comparison of the temperature increase (°C) in skin and testis at various exposure times.
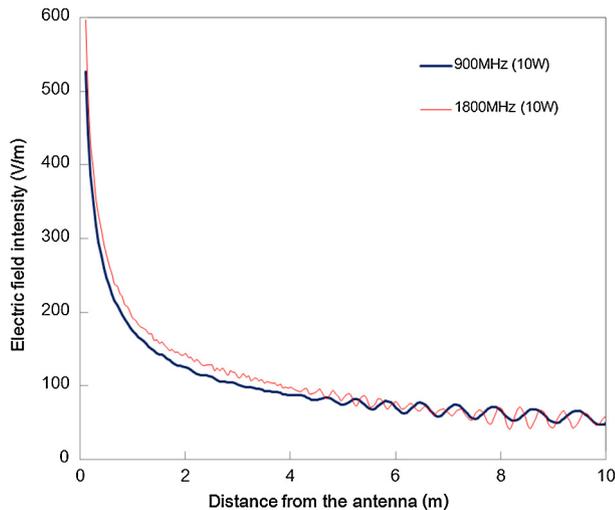

Fig. 10. The normalized electric field intensity distributions (V/m) in free space at frequencies of 900 MHz and 1800 MHz and with a radiated power of 10 W.

Fig. 8 compares the temperature increase (°C) in each tissue type that results from a radiated power of 1 W at a distance of 0.1 m (in the near-field), and 100 W at a distance of 10 m (in the far-field). For both cases, the three largest temperature increases are shown for the skin, fat, and muscle. The main reason is that the position of the skin, fat, and muscle, the outermost layers of the body, are exposed to EMF from a dipole source, where the electric field intensity is strongest. Moreover, the skin also has a high dielectric constant value (ε) and a high electrical conductivity (σ), which means that the propagating EM energy can be conducted and absorbed, which produces localized heating. From the figure, the temperature increases for the skin and fat, for the near-field case, are higher than the corresponding values in the far-field. While in other organs, the far-field case shows higher values for the temperature increase than for the parameters in the near-field. Only small temperature increases occur in the bone and in the testis. This is because the penetration area of the far-field case is wider than that of the near-field case. It is found that the temperature increase distributions in the human body are not directly proportional to the local SAR distributions. Nevertheless,

this is also related to parameters such as surface convection, thermal conductivity, dielectric properties, and the blood perfusion rate. It is found that, when the model is subjected to EM fields for different exposure conditions, the distribution patterns for the temperature are significantly different. This is because the difference in the temperature distribution patterns between the two cases is caused by dielectric properties, as well as the thermal properties of the tissue, which become the dominant mechanisms for heat transfer.

4.3. Effect of exposure time

Fig. 9 shows the comparison of the temperature increase in the testis and skin, which are sensitive organs of a human, to EMFs after various exposure times. From Fig. 9, it is found that the exposure time significantly influences the temperature increase in the testis and skin. A longer exposure time resulted in greater heat accumulation in the tissue; thereby increasing its temperature. It takes approximately 1000 seconds to a reach steady state for both the near-field and the far-field. The temperature increase of the testis at a near-field condition is found to be lower than that of the far-field over the exposure time. However, over the exposure time, the skin temperature increase in the near-field is not significantly different from that for the far-field. The results obtained in the near-field and the far-field are in agreement with the data shown in Fig. 8. It can be seen that the temperature increase varies according to the distribution of the electric fields (Fig. 5) and the SAR (Fig. 6). Due to the wider penetration of the electric field and the SAR for the far-field case, a higher temperature increase occurred in the testis than in the near-field case as shown in Fig. 9.

4.4. Effects of operating frequency and exposure distance

In this study, the effects of the operating frequency and the exposure distance are also investigated. In this part, the heterogeneous human model is exposed to a radiated power of 10 W at frequencies of 900 and 1800 MHz. To illustrate the penetrated electric field distribution in free space at different frequencies, numerical simulations of EM wave propagation are carried out. Fig. 10 shows the normalized electric field intensity distributions (V/m) in free space at frequencies of 900 MHz and 1800 MHz with a radiated power of 10 W. For both frequencies, the electric field intensity decreases exponentially in the direction of wave propagation. It
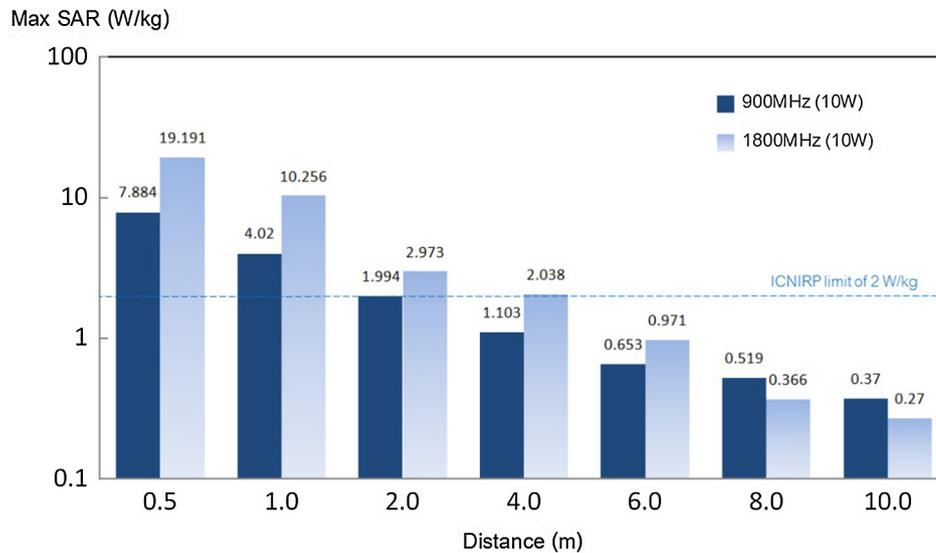
Fig. 11. Comparison of the maximum SAR (W/kg) with different antenna-body distances for the frequencies of 900 MHz and 1800 MHz.
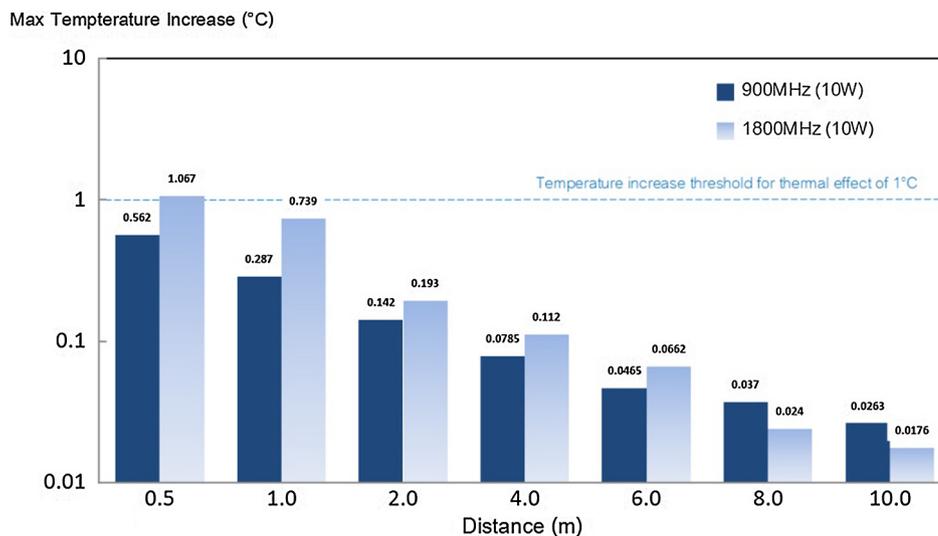

Fig. 12. Comparison of the maximum temperature increase (°C) resulting from different antenna-body distances for the frequencies of 900 MHz and 1800 MHz.

is found that the electric field strength decreases inversely with the distance from the source. The distribution curves shown are not smooth and show a wavy behavior because of the standing wave that appeared in the space. The electric field intensity near the antenna, which has a frequency of 1800 MHz, displays a value higher than 900 MHz. Conversely, at a longer distance, the lower frequency, where the 900 MHz frequency has a longer wavelength, travels further over a higher frequency due to a lower degree of attenuation.

Exposure distances between 0.5–10 m were selected to represent both typical and extreme exposure situations. Fig. 11 compares the maximum SAR values resulting from different antenna-body distances at frequencies of 900 MHz and 1800 MHz and a radiated power of 10 W. For the near-field exposures, high rates of energy absorption in the human body occur. The maximum SAR values resulting from the 1800 MHz frequency are higher than the values caused by the 900 MHz frequency for all the distances

except at 8.0 m and 10.0 m. This is because the penetration of the 900 MHz frequency is stronger than the 1800 MHz frequency for further distances, which correspond to the electric field intensity shown in Fig. 10.

Comparison of the maximum SAR value can also be analyzed from the standard setting point of view and by evaluating potential hazards that result from exposure to portable transmitters. Compared to the ICNIRP standard for the safety level, which specifies a maximum SAR value of 2 W/kg (general public exposure) [1], the resulting SAR values from both the 900 MHz and 1800 MHz frequencies, at distances less than 4.0 m and 2.0 m respectively, exceeded the recommended limit for general public exposure.

The SAR distribution shown in Fig. 11 is transformed into an incremental amount of heat through EMF absorption by the tissue. Fig. 12 shows the temperature increase in the human model upon exposure to an EMF radiated with a power of 10 W at the frequencies of 900 MHz and 1800 MHz. For the model exposed to the EMF,

the tissue temperature (Fig. 12) increase in correspondence to the maximum SAR (Fig. 11). This is because the electric fields in the tissue attenuate owing to the absorbed energy, and thereafter, the energy deposition in the tissue is converted to thermal energy, which increases the body temperature. It is found that, when the model is subjected to the EM fields at different frequencies, the maximum temperature increase at various distances is different. This is because the difference in the temperature distribution pattern between the two chosen frequencies is caused by the dielectric properties of the tissue, as well as the electric field penetration shown in Fig. 10, which becomes the dominant mechanisms for energy absorption. At a distance of 0.5 m, the maximum temperature increase in the testis exposed to a radiated power density of 10 W at frequencies of 900 and 1800 MHz are 0.562 and 1.067 °C respectively. The temperature increases that are obtained may cause a decrease in male sperm production, alter the production of hormones, and suppress a human's immune response [4,29]. Exposure to a 10 W antenna, at a distance of 0.5 m, can be considered as the worst-case representation of practical near-field radiators, and the obtained data may be used to estimate potential hazards from EM exposure. However the 2D model simplifications made in this study might affect the accuracy of the result due to the offset of the organ from the sagittal plane.

5. Conclusions

The numerical simulations of the electric field, the SAR and the temperature distributions, as performed in this study, show several important features regarding the energy absorption and the temperature increase in the heterogeneous human model during exposure to near-field and far-field EMFs with frequencies of 900 and 1800 MHz. In the model, the electric field distributions display a wavy behavior, and the energy absorbed by the organs shows a strong dependence on the exposure distance and the dielectric properties of the tissue. The distribution patterns of the SAR vary in accordance with the electric field intensities. Besides the electric field intensity, the magnitude of the dielectric and thermal properties in each tissue type will directly affect a SAR's distribution pattern. We refer to the SAR safety limit indicated in the guidelines as 2 W/kg for general public exposure, and 10 W/kg for occupational exposure according to the ICNIRP [1]. However, for distances less than 2 m, the SAR values are higher than the general public exposure limit of 2 W/kg, but they are lower than the occupational exposure limit of 10 W/kg as specified in the ICNIRP. Moreover, the calculated testis temperature increases are lower than the thresholds for the induction of infertility, which is 1 °C for both 900 and 1800 MHz at a radiated power of 10 W and exposure distances longer than 1.0 m.

The results obtained in this study may be of assistance in determining the exposure limits for the power output of wireless transmitters, mobile phones, and base stations and their interactions with humans. In future works, the effect of the feed point position will be included in the analysis to represent the actual heat transfer process, where a more realistic 3D model will be developed for the simulations. This will allow a better understanding for the real interactions between EM fields and the human body. The values obtained in this study represent the accurate phenomena and determines the temperature increase in the human body, as well as indicates the limitations that must be considered, as the temperature increases due to EM energy absorption from EM field exposure at different exposure conditions.

Conflict of interest

The authors declare that there is no conflict of interest.

References

[1] International Commission on Non-Ionizing Radiation Protection: ICNIRP, Guidelines for limiting exposure to time-varying electric, magnetic and electromagnetic fields (up to 300 GHz), Health Phys. 74 (1998) (1998) 494–522.
[2] A. Hirata, S. Matsuyama, T. Shiozawa, Temperature rises in the human eye exposed to EM waves in the frequency range 0.6–6 GHz, IEEE Trans. Electromagn. Compat. 42 (4) (2000) 386–393.
[3] O.P. Gandhi, G. Kang, Some present problems and a proposed experimental phantom for SAR compliance testing of cellular telephones at 835 MHz and 1900 MHz, Phys. Med. Biol. 47 (2002) 1501–1518.
[4] M.A. Stuchly, Health effects of exposure to electromagnetic fields, in: Proceedings of the IEEE Aerospace Applications Conference, vol. 1, 1995, pp. 351–368.
[5] H.H. Pennes, Analysis of tissue and arterial blood temperature in the resting human forearm, J. Appl. Physiol. 1 (1948) 93–122.
[6] H.H. Pennes, Analysis of tissue and arterial blood temperatures in the resting human forearm, J. Appl. Phys. 85 (1998) 5–34.
[7] W. Wulff, The energy conservation equation for living tissue, IEEE Trans. Biomed. Eng. 21 (6) (1974) 494–495.
[8] H.G. Klinger, Heat transfer in perfused biological tissue. I: General theory, Bull. Math. Biol. 36 (4) (1974) 403–415.
[9] M.M. Chen, K.R. Holmes, Microvascular contributions in tissue heat transfer, Ann. N. Y. Acad. Sci. 335 (1980) 137–150.
[10] A.M. Seufi, S.S. Ibrahim, T.K. Elmaghraby, E.E. Hafez, Preventive effect of the flavonoid, quercetin, on hepatic cancer in rats via oxidant/antioxidant activity: molecular and histological evidences, J. Exp. Clin. Cancer Res. 28 (1) (2009) 80.
[11] D. Yang, M.C. Converse, D.M. Mahvi, J.G. Webster, Measurement and analysis of tissue temperature during microwave liver ablation, IEEE Trans. Biomed. Eng. 54 (1) (2007) 150–155.
[12] H. Kanai, H. Marushima, N. Kimura, T. Iwaki, M. Saito, K. Maehashi, K. Shimizu, M. Muto, T. Masaki, K. Ohkawa, K. Yokoyama, M. Nakayama, T. Harada, H. Hano, Y. Hataba, T. Fukuda, M. Nakamura, N. Totsuka, S. Ishikawa, Y. Unemura, Y. Ishii, K. Yanaga, T. Matsuura, Extracorporeal bioartificial liver using the radial-flow bioreactor in treatment of fatal experimental hepatic encephalopathy, Artif. Organs 31 (2) (2007) 148–151.
[13] P.J. Riu, K.R. Foster, Heating of tissue by near-field exposure to a dipole, IEEE Trans. Biomed. Eng. 46 (8) (1999) 911–917.
[14] A. Ferikoğlu, O. Çerezci, M. Kahriman, Ş. Çağrı Yener, Electromagnetic absorption rate in a multilayer human tissue model exposed to base-station radiation using transmission line analysis, IEEE Antennas Wireless Propag. Lett. 13 (2014) 903–906.
[15] T. Wessapan, S. Srisawatdhisukul, P. Rattanadecho, Numerical analysis of specific absorption rate and heat transfer in the human body exposed to leakage electromagnetic field at 915 MHz and 2450 MHz, ASME J. Heat Transfer 133 (2011) 051101.
[16] T. Wessapan, S. Srisawatdhisukul, P. Rattanadecho, The effects of dielectric shield on specific absorption rate and heat transfer in the human body exposed to leakage microwave energy, Int. Commun. Heat Mass Transfer 38 (2011) 255–262.
[17] T. Wessapan, P. Rattanadecho, Numerical analysis of specific absorption rate and heat transfer in human head subjected to mobile phone radiation, ASME J. Heat Transfer 134 (2012) 121101.
[18] T. Wessapan, S. Srisawatdhisukul, P. Rattanadecho, Specific absorption rate and temperature distributions in human head subjected to mobile phone radiation at different frequencies, Int. J. Heat Mass Transfer 55 (2012) 347–359.
[19] P. Keangin, T. Wessapan, P. Rattanadecho, An analysis of heat transfer in liver tissue during microwave ablation using single and double slot antenna, Int. Commun. Heat Mass Transfer 38 (2011) 757–766.
[20] P. Rattanadecho, P. Keangin, Numerical study of heat transfer and blood flow in two-layered porous liver tissue during microwave ablation process using single and double slot antenna, Int. J. Heat Mass Transfer 58 (2013) 457–470.
[21] P. Keangin, T. Wessapan, P. Rattanadecho, Analysis of heat transfer in deformed liver cancer modeling treated using a microwave coaxial antenna, Appl. Therm. Eng. 31 (16) (2011) 3243–3254.
[22] T. Wessapan, P. Rattanadecho, Specific absorption rate and temperature increase in human eye subjected to electromagnetic fields at 900 MHz, ASME J. Heat Transfer 134 (2012) 091101.
[23] T. Wessapan, P. Rattanadecho, Specific absorption rate and temperature increase in the human eye due to electromagnetic fields exposure at different frequencies, Int. J. Heat Mass Transfer 64 (2013) 426–435.
[24] T. Wessapan, P. Rattanadecho, Influence of ambient temperature on heat transfer in the human eye during exposure to electromagnetic fields at 900 MHz, Int. J. Heat Mass Transfer 70 (2014) 378–388.
[25] T. Wessapan, P. Rattanadecho, Heat transfer analysis of the human eye during exposure to sauna therapy, Numer. Heat Transfer, Part A 68 (2015) 566–582.

[26] T. Wessapan, P. Rattanadecho, P. Wongchadakul, Effect of the body position on natural convection within the anterior chamber of the human eye during exposure to electromagnetic fields, Numer. Heat Transfer, Part A 69 (2016) 1014–1028.

[27] T. Wessapan, P. Rattanadecho, Temperature induced in the testicular and related tissues due to electromagnetic fields exposure at 900 MHz and 1800 MHz, Int. J. Heat Mass Transfer 102 (2016) 1130–1140.

[28] P.A. Hasgall, F. Di Gennaro, C. Baumgartner, E. Neufeld, M.C. Gosselin, D. Payne, A. Klingenböck, N. Kuster, IT'IS Database for thermal and electromagneticparameters of biological tissues. Version 3.0, September 1st. 2015. http://www.itis.ethz.ch/database, DOI: https://doi.org/10.13099/VIP21000-03-0.

[29] K. Kumar, A.B. Raju, A review on male fertility, Hygeia J. Drugs Med. 3 (1) (2011) 20–28.